iScience

CellPress
OPEN ACCESS

Article

Rapid detection of carcinoembryonic antigen by means of an electrochemical aptasensor

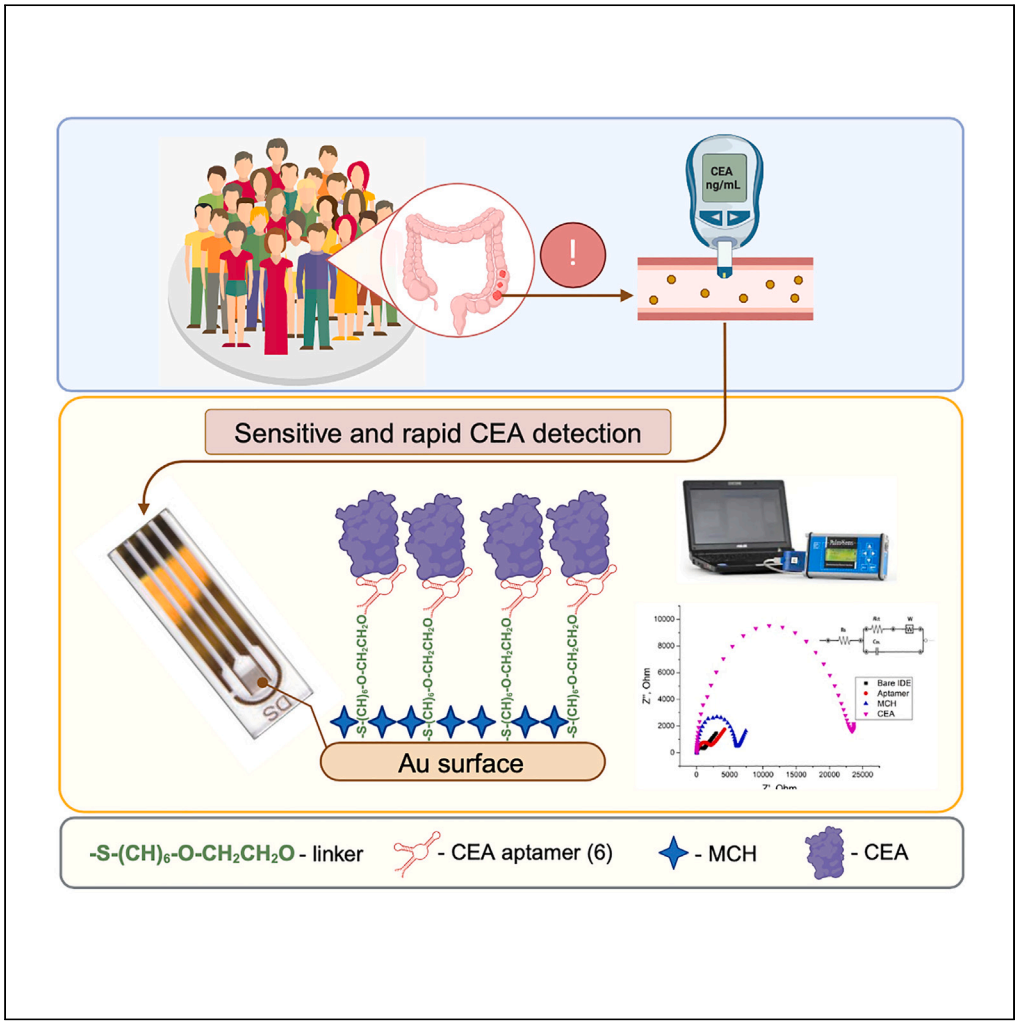

Nigara Yunussova, Meruyert Tilegen, Tri Thanh Pham, Damira Kanayeva

dkanayeva@nu.edu.kz

Highlights

A label-free EIS aptasensor for rapid and sensitive detection of CEA was developed

Detection limits of 2.4 pg/mL in buffer and 3.8 pg/mL in human serum were attained

Incubation time was 20 min, while the EIS measurements took less than 3 min

AFM validated successful target protein capture

Yunussova et al., iScience 27, 109637
May 17, 2024
https://doi.org/10.1016/j.isci.2024.109637

iScience

CellPress
OPEN ACCESS

Article

Rapid detection of carcinoembryonic antigen by means of an electrochemical aptasensor

Nigara Yunussova,[1] Meruyert Tilegen,[2] Tri Thanh Pham,[3] and Damira Kanayeva[3,4,*]

SUMMARY

Carcinoembryonic antigen (CEA) is a critical biomarker for identifying colon cancer. This work presents an electrochemical impedance spectroscopy (EIS) based aptasensor for detecting CEA, utilizing a single-stranded DNA (ssDNA) aptamer previously selected and characterized by our research group. The surface of an interdigitated gold electrode (IDE) was successfully functionalized with an 18-HEG-modified aptamer sequence. The developed aptasensor demonstrated high specificity and sensitivity with detection limits of 2.4 pg/mL and 3.8 pg/mL for CEA in buffer and human serum samples, respectively. The optimal incubation time for the target protein was 20 min, and EIS measurements took less than 3 min. Atomic force microscopy (AFM) micrographs supported the EIS data, demonstrating a change in IDE surface roughness after each modification step, confirming the successful capture of the target. The potential of this developed EIS aptasensor in detecting CEA in complex samples holds promise.

INTRODUCTION

Colorectal cancer (CRC), commonly known as colon and/or rectal cancer, is a severe public health problem since it is the third most common and second most fatal disease in the world.[1] Global CRC incidence is estimated to rise by 60% by 2035, with 2.2 million new cases and 1.1 million deaths occurring yearly.[2,3] CRC is a condition that affects the colon or rectum and is caused by the abnormal growth of glandular epithelial cells in the colon.[4] Among the most often utilized screening treatments for CRC are endoscopic exams of the large intestine (particularly flexible sigmoidoscopy and colonoscopy) and stool tests such as fecal occult blood test (FOBT). However, the aforementioned screening technologies have tangible shortcomings, such as invasiveness, low specificity and sensitivity, the need for trained personnel, and high cost.[5] The use of tumor biomarkers, such as carcinoembryonic antigen (CEA), not only aids in cancer detection but also plays a crucial role in cancer screening, prognosis, and early detection of recurrence or spread, helping to overcome this burden. CEA is a cell adhesion glycoprotein with a molecular weight of 70 kDa that increases to 180 kDa when glycosylated. It can be identified in various body samples, with widely used tumor tissue and blood and urine samples predominantly noninvasive.[6,7] Modern advances in electronics, sensor technology, and microfluidics applications have enabled device miniaturization and testing of various analytes.[8] Thus, CEA can be directly tested using a small device known as an electrochemical biosensor, which can respond continuously, reversibly, and without causing any disruption to a sample. Electrochemical biosensors combine the analytical power of electrochemical techniques with the specificity of biological recognition processes, relying on selective interactions between a target compound and a recognition element (enzyme, antibody, aptamer, tissue, or other biomolecules) to create an electrical signal proportional to the concentration of an analyte.[9–11] Most biosensors proposed for CEA detection today predominantly rely on antibodies as biorecognition elements.[12] Aptamers are synthetic single-stranded deoxyribonucleic (ssDNA) or ribonucleic acid (RNA)[13] molecules used as target identifiers in sensing platforms as well.[14] They offer advantages over the antibodies, such as thermal stability, ease of synthesis and modification, and cost-effectiveness.[15–17]

Electrochemical impedance spectroscopy (EIS) is an established method for measuring an electrical system's impedance characteristics, typically sinusoidal, at various frequencies of an applied disturbance.[18,19] The minimal and non-interfering nature of the stimulus sinusoidal voltage with most biorecognition layers is a significant benefit of EIS biosensors.[20] EIS is a label-free and sensitive detection technique that allows downsizing[21] and integrating interdigitated electrodes (IDEs) that consist of two separate arrays of microelectrodes.[22] The primary characteristic of an IDE is a gap (distance) between two individual microelectrodes arranged in an interdigitated structure; that is, the gap is less than 50 μm, which is less than the diffusion layer formed on the anode and cathode during the redox reaction. Consequently, the response at the counter electrode will maintain the decreased mediator concentration on the working electrode (WE), which is almost constant if every single microelectrode of an IDE is utilized as both a working and a counter electrode. As a result, the current will reach a steady state right away, and the sensor will display a high electric current.[22] They are one of the most used transducers in technical applications, particularly in biological and chemical sensors, because of their low cost, simplicity of manufacture, and great sensitivity.[23]

[1]Ph.D. program in Life Sciences, Department of Biology, School of Sciences and Humanities, Nazarbayev University, 53 Kabanbay batyr Avenue, Astana 010000, Kazakhstan
[2]M.Sc. program in Molecular Medicine, School of Medicine, Nazarbayev University, 5/1 Kerey-Zhanibek Khandar St, Astana 010000, Kazakhstan
[3]Department of Biology, School of Sciences and Humanities, Nazarbayev University, 53 Kabanbay batyr Avenue, Astana 010000, Kazakhstan
[4]Lead contact
*Correspondence: dkanayeva@nu.edu.kz
https://doi.org/10.1016/j.isci.2024.109637

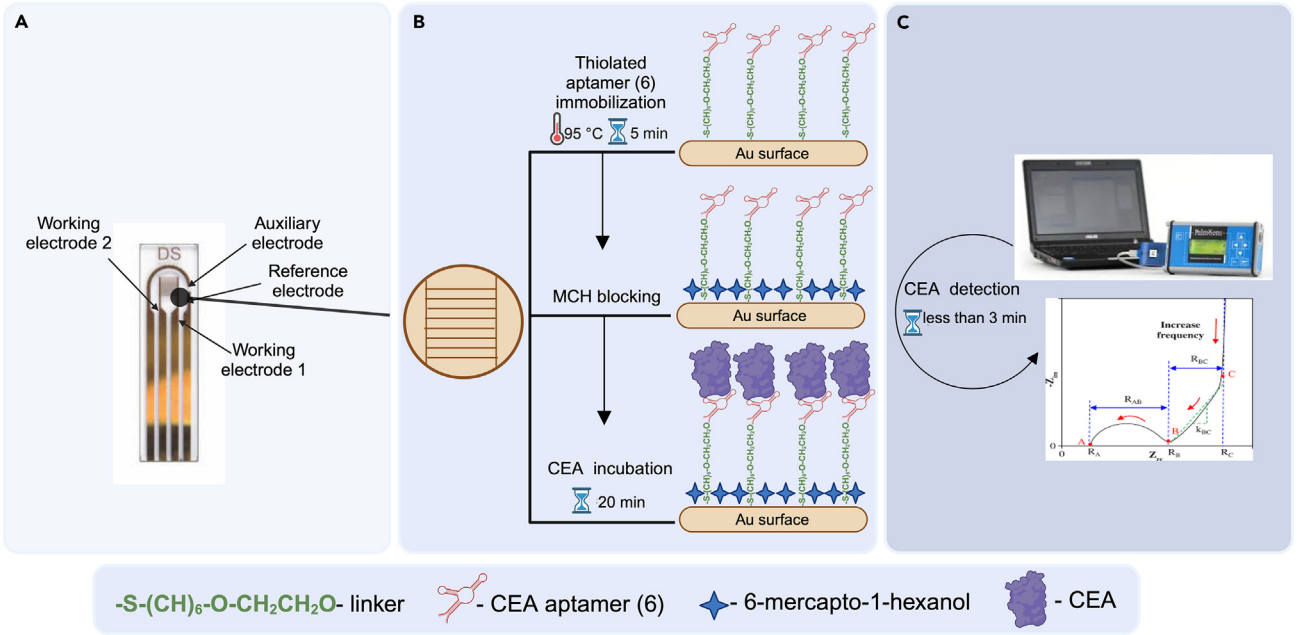

Figure 1. A schematic overview of the EIS aptasensor for CEA detection

(A) An IDE's overall structure consists of gold, two working electrodes, an auxiliary electrode, and a reference electrode, all made of the same material on a glass substrate.

(B) IDE surface functionalization steps and CEA target incubation.

(C) Measurements of EIS signals after each IDE surface modification step and the detection of the target CEA using a potentiostat and a portable computer.

One example of an electrochemical aptasensor is demonstrated in a study,[24] where graphene ink and graphene and poly (3,4-ethylenedioxythiophene): poly(styrenesulfonate (PEDOT:PSS) were gradually applied to a paper substrate to create a conductive composite paper electrode. An electrochemical aptasensor for the detection of CEA was developed with a limit of detection (LOD) of 0.45 ng/mL in a buffer and 1.06 ng/mL in a serum. The fabricated paper-based device validated the sensitivity and specificity of electrochemical measurements for CEA in serum samples, employing aptamers for immobilization. Shekari et al.[25] developed a sensitive sandwich-type electrochemical aptasensor for CEA detection using a hemin-G4-based signal amplification technique. The electrode surface was modified with nitrogen-doped graphene (NG), gold nanoparticles (AuNPs), and graphene quantum dots (GQDs) that allowed the detection of CEA in human serum samples with an LOD for CEA in a buffer that was found to be 3.2 fg/mL. These studies suggest that enhancing the sensitivity of aptasensors and exploring the development of a label-free EIS aptasensor could significantly reduce detection time, providing a cost-effective approach.

Here, we developed a novel label-free EIS-based aptasensor for detecting CEA in a buffer and human serum. Figure 1 illustrates the workflow of the EIS aptasensor fabrication and the subsequent CEA detection process. The bare IDE surface was first modified using a thiolated CEA aptamer (6) sequence, which our research team previously selected and characterized.[26] In the current study, the ssDNA aptamer sequence (6) with a total length of 39 nucleotides underwent modification with the addition of a linker in the form of $HS(CH_6)_6$-$OP(O)_2O$-$(CH_2CH_2O)_6$-5′-TTTTT- aptamer (6) -3′. Following this step, the IDE surface was backfilled with 6-mercapto-1-hexanol (MCH) to act as a co-immobilizing agent, thereby reducing non-specific binding. Using an IDE in this study was primarily due to its integrated electrochemical setup, eliminating the need for additional electrodes. This novel aptasensing technique that is quick, label-free, and user-friendly incorporates a newly designed CEA aptamer and successfully detects CEA in both buffer and serum samples. Validation was also carried out using atomic force microscopy (AFM) and cyclic voltammetry (CV), and the results aligned with the EIS findings.

RESULTS AND DISCUSSION

Electrochemical characterization

After each modification step, the CV and EIS measurements were carried out to characterize the electrode's interface properties.[27] Figure 2 illustrates the EIS and CV results for the IDE at different surface modification stages. Both EIS and CV measurements were performed in the presence of a dissolved 2 mM ferro/ferricyanide $[Fe(CN)_6]^{3-/4-}$ redox pair, which served as the redox mediator. Figure 2A presents a typical Nyquist plot of IDE surface functionalization steps. The Nyquist plots collect and display the generated solution resistance (R_s), charge transfer resistance (R_{ct}), and Warburg impedance (W).[28] Each point on the Nyquist plot represents an impedance value at a particular frequency. The diameter of the semicircular Nyquist plot often serves as an approximation for the R_{ct}.[29] At the x-axis, impedance was measured at low frequencies on the right side of the plot, while higher frequencies corresponded to impedances plotted on the left.[28] CV is a well-known and

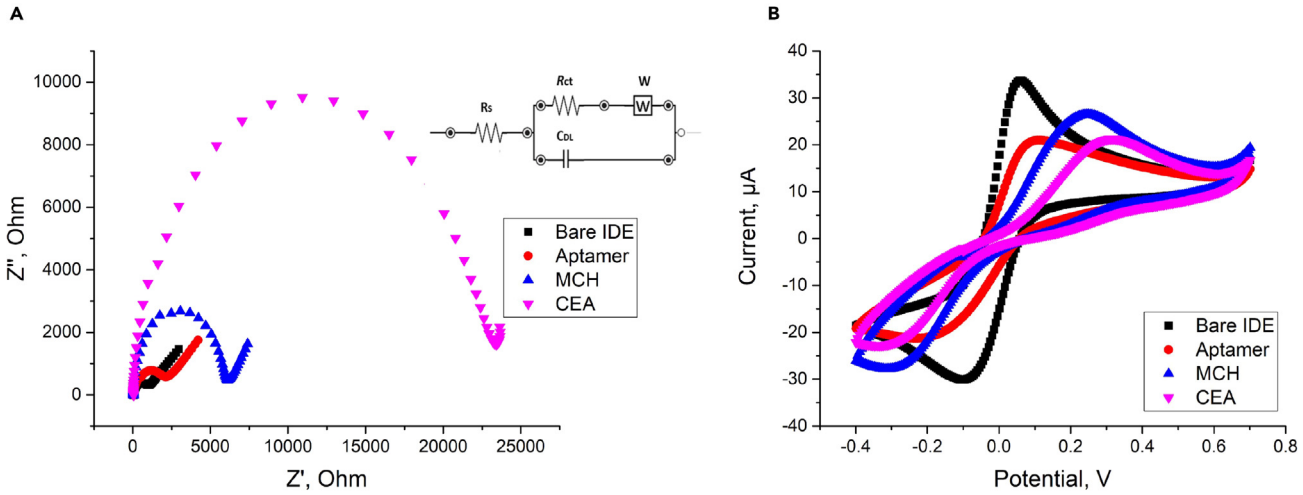

Figure 2. Characterization of an IDE surface with EIS and CV

(A) A typical Nyquist plot and (B) a cyclic modification voltammogram of a bare IDE surface, a 4 h aptamer incubation, backfilling with MCH, and the target CEA incubation (2 ng/mL). The inset in (A) shows the Randles equivalent circuit employed to model the EIS data, where R_s is the solution resistance, R_{ct} is the charge transfer resistance, C_{dl} is the double-layer capacitance, and W is the Warburg element. The experiment was conducted in three biological replicates. All data are shown as the means of ± SEMs.

versatile electrochemical method commonly used to evaluate the redox status of molecular species.[30,31] It measures the current response to a voltage applied to the sample using a WE.[31]

As can be seen from Figure 2A, the bare IDE surface exhibited a small semicircle (R_{ct} = 857 Ω). Additionally, in the voltammogram provided in Figure 2B, the highest peak current value was recorded due to the absence of an electron transfer-resistant material. Then, the semicircle steadily increased when CEA aptamer (6) was immobilized at concertation of 5 µM (R_{ct} = 1716 Ω) as the result of the redox buffer's negative electroactive ions rejecting the negatively charged phosphate groups of the DNA aptamer, confirming its attachment to the surface,[32–34] which is consistent with the CV data, where the cathode peak and anode peak decreased after fixing the aptamer because the negatively charged phosphoric acid backbones of aptamer impede the electron transfer of the redox couple.[27,35] Further blocking with MCH solution resulted in the charge transfer resistance change (R_{ct} = 5333 Ω), following CV peak currents decrease because MCH could form an additional barrier on the surface of the IDE and confirm the filling of free surface on the IDE surface. Finally, the R_{ct} increased to 19,457 Ω, when incubated with a 2 ng/mL CEA target protein for 20 min. The peak current depicted in the voltammogram decreased with the CEA immobilization since the hydrophobic layer of the protein could greatly hinder the conductivity.[36] Randles equivalent circuit model, as illustrated in Figure 2A inset, was chosen to fit the experimental data. In this model, R_s was connected in series with the double-layer capacitance C_{dl} and parallel with the R_{ct} of the surface, along with the inclusion of W to account for diffusion.

EIS aptasensor optimization studies

To ensure the sensitivity and accuracy of the EIS aptasensor for detecting CEA and to conserve reagents, it was necessary to optimize various parameters, including aptamer concentration and protein incubation time. All experimental conditions were the same as described in Section Fabrication of the EIS aptasensor and CEA detection, except aptamer concentration and protein incubation time. The results of the aptamer concentration optimization study are presented in Figure 3A. The response values of R_{ct} change increased with the concentration of CEA aptamer. Aptamer concentrations of 5 µM or higher resulted in a considerably greater R_{ct} change response (>20%) compared to 2 µM and 4 µM ($0.01 < p < 0.05$). However, there was no statistically significant difference between 5 µM and 8 µM concentrations, suggesting that the R_{ct} change is saturated at 5 µM. Therefore, the most effective aptamer concentration for target protein detection in the present study was determined to be 5 µM. Further, the incubation time for the target CEA was optimized by varying the incubation period while maintaining a constant CEA value (2 pg/mL), as shown in Figure 3B. The data also revealed that the R_{ct} response is saturated for any incubation duration of 20 min or more. The results showed that a 20-min incubation period was the optimal incubation period for the target protein to achieve an R_{ct} change response value > 20% ($0.001 < p < 0.01$). Thus, for all subsequent experiments conducted throughout this work, an aptamer concentration of 5 µM and an incubation period of 20 min were used.

Analytical performance of the EIS aptasensor

Following the optimization of parameters, target CEA was detected as described in Section Fabrication of the EIS aptasensor and CEA detection. The results of the sensitivity study for CEA diluted in a buffer (phosphate-buffered saline (PBS), pH 7.6, 10 mM) are illustrated in Figure 4A. An increase in the R_{ct} change was observed upon increasing CEA concentrations (one sample t test; p = 0.0014). The lowest concentration, 0.002 pg/mL, exhibited a 9.34% change in R_{ct}. At the highest CEA concentration of 2 ng/mL, there was a 45% change in R_{ct}. Based on the

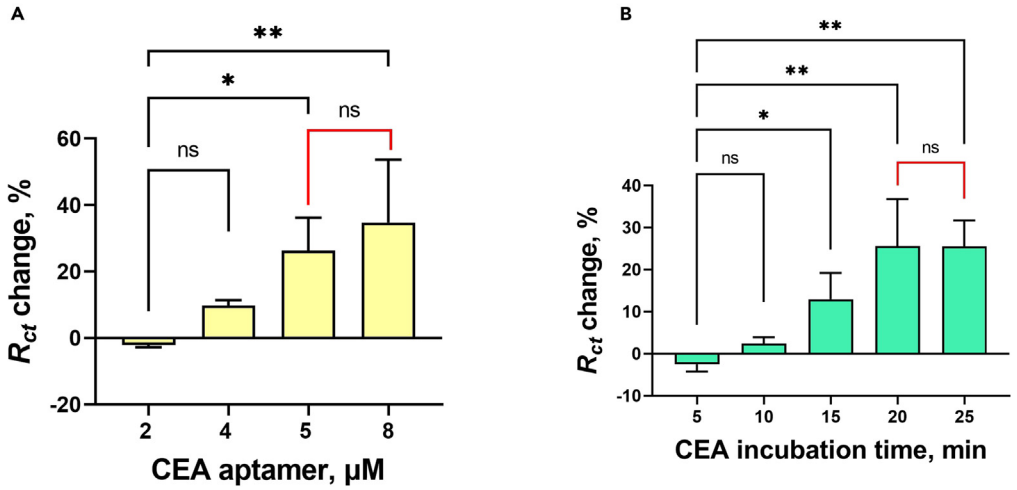

Figure 3. Optimization of experimental parameters

(A) CEA aptamer concentration optimization study. *$p \leq 0.05$, ** $0.001 < p < 0.01$.

(B) Target CEA incubation time optimization study, where target protein concentration was 2 pg/mL *$p \leq 0.05$, ** $0.001 < p < 0.01$. Experiments were conducted in at least three biological replicates. All data are shown as the means ± SEMs.

collected data, the R_{ct} change values showed a linear correlation (R^2 = 91%) with the concentration of CEA in the range from 0.002 ng/mL to 2 ng/mL, described by the regression equation $y = 5.9899x + 4.7077$, where x represents CEA concentration, and y represents the R_{ct} value (Figure 4A inset). All R_{ct} values were subtracted from the background (PBS, pH 7.6, 10 mM). The developed aptasensor showed a sensitivity with an LOD of 2.4 pg/mL within a detection range of 2 pg/mL to 2 ng/mL in a buffer. The high sensitivity and specificity of the EIS aptasensor developed in this study were primarily attained through the utilization of the CEA aptamer sequence (6), selected and characterized in our previous study.[26] Adding linkers and five thymine residues to the aptamer created space between it and the surface, facilitating its folding and enhancing its ability to bind to the protein.[37,38] Ethylene oxide (CH_2CH_2O), a hydrophilic component of the linker, was crucial in extending the aptamer away from the surface monolayer, thereby preventing steric interference with protein binding.[37,38] The IDE geometry, including factors like electrode gap width, could have also affected the sensitivity of the developed impedimetric aptasensor, contributing to its improved sensitivity.

It was crucial to assess the functionality of the aptasensor under conditions that closely resemble real-world scenarios, as the device is intended for serum-based applications. The experimental procedure for detecting CEA spiked in serum mirrored the procedure used for

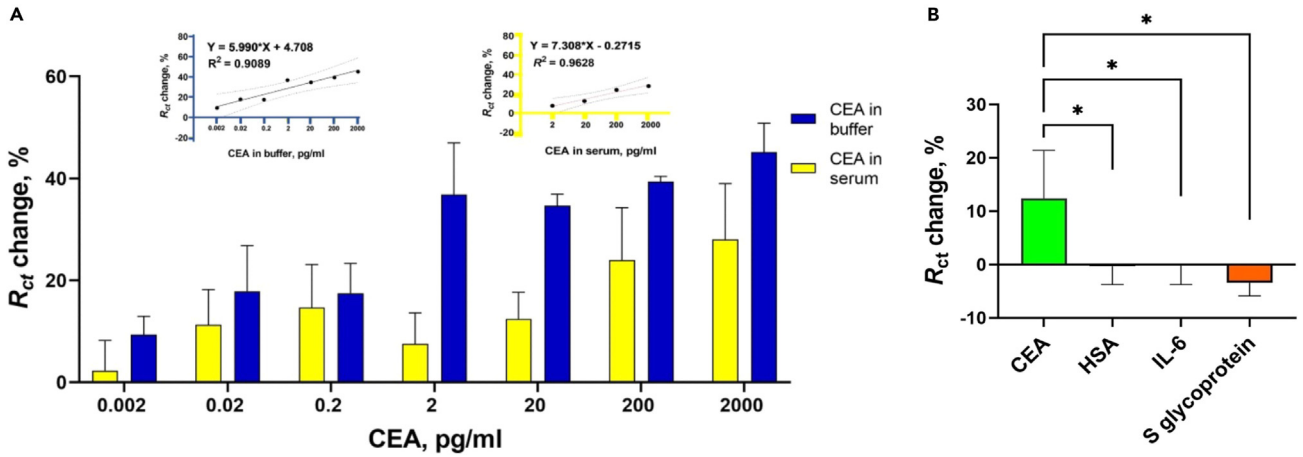

Figure 4. Analytical performance of the developed EIS aptasensor

(A) Concentration-dependent analysis of the EIS aptasensor for CEA detection in a buffer and serum. The insets show the calibration curve from 0.002 to 2000 pg/mL for buffer and from 2 to 2000 pg/mL for serum. The experiment was conducted in nine biological replicates.

(B) Specificity of the EIS aptasensor. Target CEA and non-target proteins, IL-6, HSA, and S glycoprotein of SARS CoV-2, were tested at 7 pg/mL. The experiment was conducted in three biological replicates. Data are shown as means ± SEMs (* $0.01 < p < 0.05$). All EIS measurements were recorded in a 2 mM ferro/ferricyanide $[Fe(CN)_6]^{3-/4-}$ redox couple.

buffer, with the only difference being the substitution of PBS for serum in the CEA dissolution process (Figure 4A). The R_{ct} change exhibited a linear increase (R^2 = 96%) (one sample *t* test; $p = 0.0333$) across a concentration range from 2 pg/mL to 2 ng/mL (Figure 4A inset), characterized by the regression equation of $y = 7.308x–0.2715$, where x represents the CEA concentration, and y represents the R_{ct} change value. The LOD for the EIS aptasensor in detecting CEA in spiked serum samples was determined to be 3.8 pg/mL, achieved through affinity, specificity, and specific modifications incorporated into the aptamer (6) as described earlier for the LOD in the detection of CEA in the buffer. The presence of impurities and other proteins in serum samples could impact the binding of the target protein to the aptamer, resulting in lower R_{ct} change values. The normal range for CEA in the blood is 0–2.5 ng/mL,[12,39] with levels above 10 ng/mL suggesting a severe disease and levels exceeding 20 ng/mL indicating potential malignancy development.[40,41] Summarizing the data in Table S1, our aptasensor's LOD aligns with or exceeds that of already published aptasensors with improved detection time (less than 30 min). Therefore, our current approach demonstrates the aptitude to detect CEA within the clinically relevant ranges while being rapid.

In this research, we also evaluated the response of the developed EIS aptasensor to non-target proteins, including human serum albumin (HSA), interleukin-6 (IL-6), and severe acute respiratory syndrome coronavirus 2 (SARS-CoV-2) spike (S) glycoprotein, using the developed EIS aptasensor. The specificity test results are shown in Figure 4B. Unlike the three interfering proteins, the EIS aptasensor exhibited a significant R_{ct} change response only to CEA. The R_{ct} change for CEA equaled 12.4%, whereas the R_{ct} change values for non-target proteins were negative. The experimental procedure was identical to that used for CEA, except for the non-target proteins. We selected these non-target proteins for specific reasons. HSA, a liver-produced globular protein with a molecular weight of 66.5 kDa,[42,43] stands as the most abundant plasma protein (35–50 mg/mL) in blood, maintaining stable blood pH and osmotic pressure.[44] IL-6, a cytokine that promotes inflammation and plays a role in the growth and development of human cells, also triggers the release of several proteins causing acute inflammation.[45] Additionally, we included S glycoprotein for specificity testing, which is responsible for binding to the human angiotensin-converting enzyme 2 (ACE2) and initiating viral entry into host cells.[46–49]

Characterization of an IDE surface morphology

AFM is a relatively recent technology for studying local surface features at length scales ranging from submicron to nanoscale.[50] A cantilever with a molecularly sharp probe at its end, several micrometers in length, is used to trace the topography of the sample and measure forces between the probe and sample with piconewton sensitivity.[51] Because of its ability to image at such tiny scales, compact size, and ease of use, AFM is one of the few instruments capable of characterizing surface characteristics around extremely small structures.[50] Figures 5A–5E shows the surface morphology of all functionalization phases of an IDE surface, including the bare electrode. Figure 5F depicts the root-mean-square roughness of the IDE surface during all functionalization and detection stages. As can be seen, the surface of the bare IDE in Figure 5A is relatively smooth, with a measured roughness of 1.62 $\pm$ 0.04 nm. The roughness increased to 2.16 $\pm$ 0.05 nm following aptamer treatment (Figure 5B). However, when the aptamer-treated surface was functionalized with the blocking agent, MCH, the roughness dropped to a value close to the bare electrode, measuring 1.74 $\pm$ 0.05 nm (Figure 5C). The reduction was due to MCH filling in the valleys created by aptamers, which also lowers the height difference between the highest and the lowest points on the surface.

Subsequent treatment with CEA in PBS (pH 7.6, 10 mM) (Figure 5D) and serum (Figure 5E), the roughness increased to 2.67 $\pm$ 0.07 nm and 3.31 $\pm$ 0.16 nm, respectively. These results confirm the successful attachment of protein molecules to the aptamer. Surprisingly, the surface of the CEA in the serum step had a higher roughness, suggesting either that the CEA in serum forms aggregates or that other components in serum bind to the surface-bound aptamers. To validate this hypothesis, a custom-written MATLAB code was used to quantify the size and shape of micelles formed on the electrode surface for each functionalization step, as illustrated in Figure S1. Figure 5G shows the micelle cross-sectional area for all steps, with the CEA in serum having the largest micelle area. Figure 5H demonstrates that micelles from most stages, except for CEA in serum, are somewhat circular because their circularity ($C = 4\pi A/P^2$, where A is the area and P is the perimeter) values are close to 1.

To sum up, we successfully developed a novel, label-free EIS-based aptasensor for rapid and sensitive detection of CEA. Our sensing strategy achieved a 2.4 pg/mL detection limit for CEA within the detection range of 2 pg/mL to 2 ng/mL in a buffer. Furthermore, when applied to human serum, our aptasensor successfully detected CEA with a detection limit of 3.8 pg/mL within a short incubation time of 20 min and a detection time of 2.5 min, highlighting its diagnostic potential. Moreover, the aptasensor demonstrated specific binding to CEA compared to non-target proteins, emphasizing the achieved selectivity resulting from the specificity of the aptamer sequence (6) previously selected by our group and the IDE surface chemistry. AFM analysis of the IDE surface validated our findings. Our aptasensor's detection limit, as shown in Table S1, is consistent with previously reported aptasensors and offers a promising alternative for detecting colon cancer. Future work will evaluate the aptasensor's analytical performance in clinical samples and optimize the blocking procedure by employing different solutions.

Limitations of the study

When testing spiked human serum samples, there is a potential for cross-reaction with other proteins. In such cases, gold nanoparticles (AuNPs) can enhance the detection signal. Another approach is to utilize a sandwich assay with our selected aptamers and increase detection sensitivity.

STAR★METHODS

Detailed methods are provided in the online version of this paper and include the following:

- KEY RESOURCES TABLE
- RESOURCE AVAILABILITY

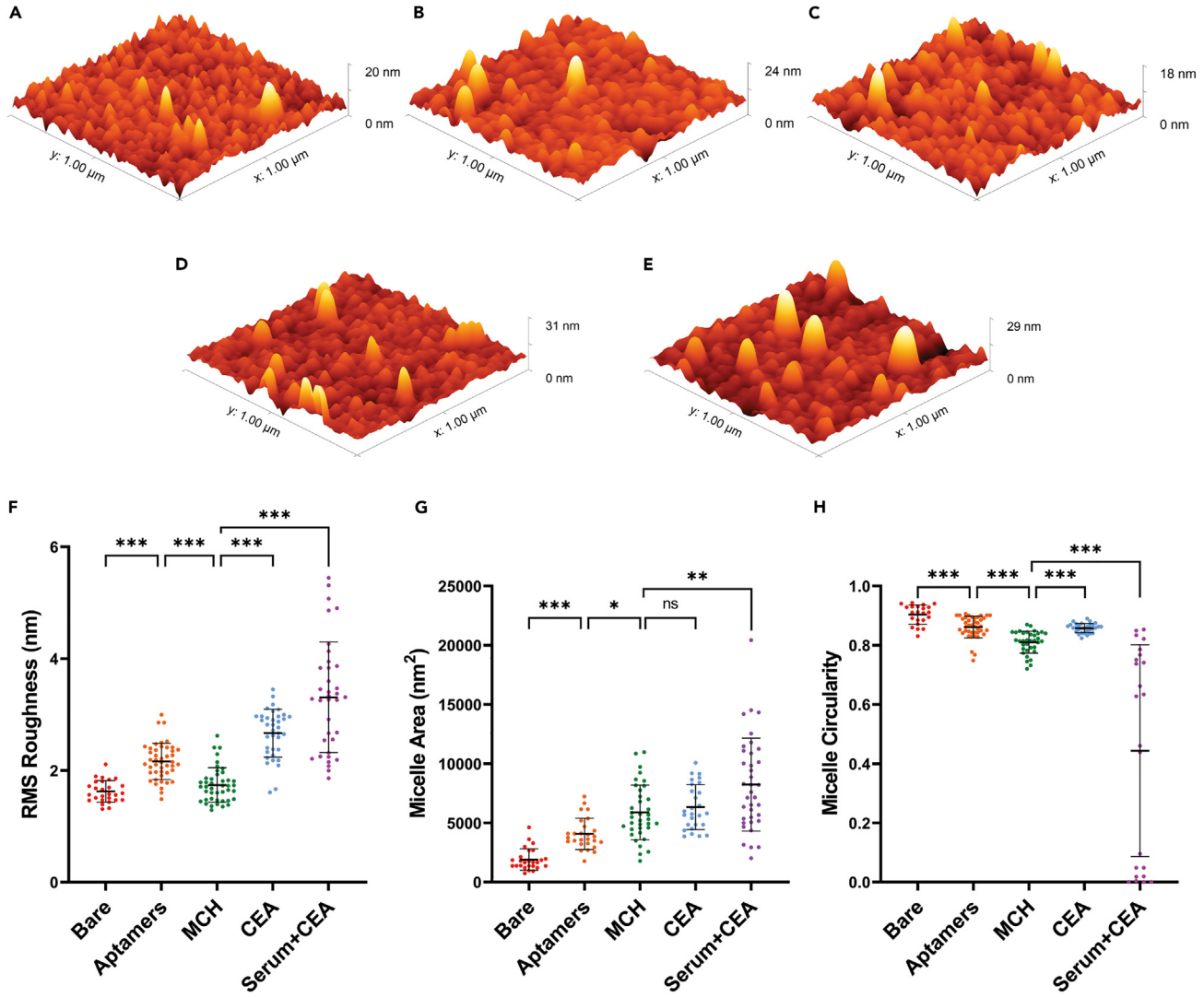

Figure 5. Analysis of surface morphology for bare and modified electrodes

Representative 3D images of a 1 μm^2 scanned electrode surface for (A) bare electrode, (B) treatment with the aptamer, (C) blocking with MCH, (D) treatment with CEA in PBS, and (E) treatment of CEA in serum. (F) Comparison of roughness for all functionalization steps ($N \geq 30$). Micelle area (G) and circularity (H) are statistically compared after each functionalization step (* $0.01 < p < 0.05$, ** $0.001 < p < 0.01$, *** $p < 0.001$).

- Lead contact
- Materials availability
- Data and code availability

- METHOD DETAILS
  - Fabrication of the EIS aptasensor and CEA detection
  - Electrochemical measurements
  - Optimization studies
  - Specificity study
  - Detection of CEA in serum
  - AFM study

- QUANTIFICATION AND STATISTICAL ANALYSIS

SUPPLEMENTAL INFORMATION

Supplemental information can be found online at https://doi.org/10.1016/j.isci.2024.109637.

ACKNOWLEDGMENTS

This research was funded by the Science Committee of the Ministry of Science and Higher Education (MSHE) of the Republic of Kazakhstan (grants AP19679890 and AP08053347). We also acknowledge the MSHE of the Republic of Kazakhstan for their scholarship support of N.Y. and M.T. for their studies at Nazarbayev University (Kazakhstan). We want to thank Assem Kurmangali and Michael Shola-David for their assistance in preparing samples for AFM measurements.

AUTHOR CONTRIBUTIONS

Conceptualization, D.K., and N.Y.; methodology, N.Y., M.T., T.T.P., and D.K.; investigation, N.Y. and M.T.; software, T.T.P.; writing – original draft, N.Y., T.T.P., and D.K.; writing – review & editing, D.K. and T.T.P.; supervision, D.K.; project administration, D.K.; funding acquisition, D.K.

DECLARATION OF INTERESTS

The authors declare no competing interests.

Received: November 7, 2023
Revised: February 3, 2024
Accepted: March 26, 2024
Published: March 28, 2024

REFERENCES

1. World Health Organization (WHO): Cancer. [Accessed 2023 July 9]. https://www.who.int/news-room/fact-sheets/detail/cancer.
2. Arnold, M., Sierra, M.S., Laversanne, M., Soerjomataram, I., Jemal, A., and Bray, F. (2017). Global patterns and trends in colorectal cancer incidence and mortality. Gut *66*, 683–691. https://doi.org/10.1136/gutjnl-2015-310912.
3. Bray, F., Ferlay, J., Soerjomataram, I., Siegel, R.L., Torre, L.A., and Jemal, A. (2018). Global cancer statistics 2018: Globocan estimates of incidence and mortality worldwide for 36 cancers in 185 countries. CA A Cancer J. Clin. *68*, 394–424. https://doi.org/10.3322/caac.21492.
4. Hossain, M.S., Karuniawati, H., Jairoun, A.A., Urbi, Z., Ooi, D.J., John, A., Lim, Y.C., Kibria, K.M.K., Mohiuddin, A.K.M., Ming, L.C., et al. (2022). Colorectal cancer: A review of carcinogenesis, global epidemiology, current challenges, risk factors, preventive, and treatment strategies. Cancers *14*, 1732. https://doi.org/10.3390/cancers14071732.
5. Mármol, I., Sánchez-de-Diego, C., Pradilla Dieste, A., Cerrada, E., and Rodriguez Yoldi, M.J. (2017). Colorectal carcinoma: A general overview and future perspectives in colorectal cancer. Int. J. Mol. Sci. *18*, 197. https://doi.org/10.3390/ijms18010197.
6. Altintas, Z., and Tothill, I. (2013). Biomarkers and biosensors for the early diagnosis of lung cancer. Sensor. Actuator. B Chem. *188*, 988–998. https://doi.org/10.1016/j.snb.2013.07.078.
7. Cui, F., Zhou, Z., and Zhou, H.S. (2020). Review—measurement and analysis of cancer biomarkers based on electrochemical biosensors. J. Electrochem. Soc. *167*, 037525. https://doi.org/10.1149/2.0252003jes.
8. Uludag, Y., Narter, F., Sağlam, E., Köktürk, G., Gök, M.Y., Akgün, M., Barut, S., and Budak, S. (2016). An integrated lab-on-a-chip-based electrochemical biosensor for rapid and sensitive detection of cancer biomarkers. Anal. Bioanal. Chem. *408*, 7775–7783. https://doi.org/10.1007/s00216-016-9879-z.
9. Malhotra, B.D., Kumar, S., and Pandey, C.M. (2016). Nanomaterials based biosensors for cancer biomarker detection. J. Phys, Conf. Ser. *704*, 012011. https://doi.org/10.1088/1742-6596/704/1/012011.
10. Xiang, W., Lv, Q., Shi, H., Xie, B., and Gao, L. (2020). Aptamer-based biosensor for detecting carcinoembryonic antigen. Talanta *214*, 120716. https://doi.org/10.1016/j.talanta.2020.120716.
11. Lv, S., Zhang, K., Zhu, L., Tang, D., Nießner, R., and Knopp, D. (2019). H2-Based Electrochemical Biosensor with Pd Nanowires@ZIF-67 Molecular Sieve Bilayered Sensing Interface for Immunoassay. Anal. Chem. *91*, 12055–12062. https://doi.org/10.1021/acs.analchem.9b03177.
12. Truta, L.A., and Sales, M.G.F. (2019). Carcinoembryonic antigen imprinting by electropolymerization on a common conductive glass support and its determination in serum samples. Sensor. Actuator. B Chem. *287*, 53–63. https://doi.org/10.1016/j.snb.2019.02.033.
13. Khan, N.I., and Song, E. (2020). Lab-on-a-Chip systems for Aptamer-Based biosensing. Micromachines *11*, 220. https://doi.org/10.3390/mi11020220.
14. Kaur, H., Bruno, J.G., Kumar, A., and Sharma, T.K. (2018). Aptamers in the therapeutics and diagnostics pipelines. Theranostics *8*, 4016–4032. https://doi.org/10.7150/thno.25958.
15. Douaki, A., Garoli, D., Inam, A.K.M.S., Angeli, M.a.C., Cantarella, G., Rocchia, W., Wang, J., Petti, L., and Lugli, P. (2022). Smart approach for the design of highly selective Aptamer-Based biosensors. Biosensors *12*, 574. https://doi.org/10.3390/bios12080574.
16. Qiu, Z., Shu, J., and Tang, D. (2017). Bioresponsive Release System for Visual Fluorescence Detection of Carcinoembryonic Antigen from Mesoporous Silica Nanocontainers Mediated Optical Color on Quantum Dot-Enzyme-Impregnated Paper. Anal. Chem. *89*, 5152–5160. https://doi.org/10.1021/acs.analchem.7b00989.
17. Zhang, K., Lv, S., Zhou, Q., and Tang, D. (2020). CoOOH nanosheets-coated g-C3N4/CuInS2 nanohybrids for photoelectrochemical biosensor of carcinoembryonic antigen coupling hybridization chain reaction with etching reaction. Sensor. Actuator. B Chem. *307*, 127631. https://doi.org/10.1016/j.snb.2019.127631.
18. Zamfir, L.-G., Puiu, M., and Bala, C. (2020). Advances in electrochemical impedance spectroscopy detection of endocrine disruptors. Sensors *20*, 6443. https://doi.org/10.3390/s20226443.
19. Brett, C.M.A. (2022). Electrochemical impedance spectroscopy in the characterisation and application of modified electrodes for electrochemical sensors and biosensors. Molecules *27*, 1497. https://doi.org/10.3390/molecules27051497.
20. Li, H., Liu, X., Li, L., Mu, X., Genov, R., and Mason, A.J. (2016). CMOS electrochemical instrumentation for Biosensor Microsystems: A Review. Sensors *17*, 74. https://doi.org/10.3390/s17010074.
21. Bahadır, E.B., and Sezgintürk, M.K. (2016). A Review on Impedimetric Biosensors. Artif. Cells, Nanomed. Biotechnol. *44*, 248–262. https://doi.org/10.3109/21691401.2014.942456.
22. Hatada, M., Loew, N., Okuda-Shimazaki, J., Khanwalker, M., Tsugawa, W., Mulchandani, A., and Sode, K. (2021). Development of an interdigitated Electrode-Based Disposable Enzyme Sensor strip for glycated albumin measurement. Molecules *26*, 734. https://doi.org/10.3390/molecules26030734.
23. Mazlan, N.S., Ramli, M.M., Abdullah, M.M., Halin, D.S.C., Isa, S.S.M., Talip, L.F.A., Danial, N.S., and Murad, S.A.Z. (2017). Interdigitated electrodes as impedance and capacitance biosensors: A review. In AIP Conference proceedings. https://doi.org/10.1063/1.5002470.
24. Yen, Y.K., Chao, C.H., and Yeh, Y.S. (2020). A Graphene-PEDOT: PSS Modified Paper-Based Aptasensor for Electrochemical Impedance Spectroscopy Detection of Tumor Marker. Sensors *20*, 1372. https://doi.org/10.3390/s20051372.
25. Shekari, Z., Zare, H.R., and Falahati, A. (2019). Electrochemical sandwich aptasensor for the carcinoembryonic antigen using graphene quantum dots, gold nanoparticles and nitrogen doped graphene modified electrode and exploiting the peroxidase-mimicking activity of a G-quadruplex

DNAzyme. Mikrochim. Acta *186*, 530. https://doi.org/10.1007/s00604-019-3572-9.
26. Yunussova, N., Sypabekova, M., Zhumabekova, Z., Matkarimov, B., and Kanayeva, D. (2022). A Novel ssDNA Aptamer Targeting Carcinoembryonic Antigen: Selection and Characterization. Biology *11*, 1540. https://doi.org/10.3390/biology11101540.
27. Zhang, Q., Fan, G., Chen, W., Liu, Q., Zhang, X., Zhang, X., and Liu, Q. (2020). Electrochemical sandwich-type thrombin APTASENSOR based on dual signal amplification strategy of silver nanowires and hollow Au-CeO2. Biosens. Bioelectron. *150*, 111846. https://doi.org/10.1016/j.bios.2019.111846.
28. Magar, H.S., Hassan, R.Y.A., and Mulchandani, A. (2021). Electrochemical Impedance Spectroscopy (EIS): principles, construction, and biosensing applications. Sensors *21*, 6578. https://doi.org/10.3390/s21196578.
29. Zeng, R., Qiu, M., Wan, Q., Huang, Z., Liu, X., Tang, D., and Knopp, D. (2022). Smartphone-Based Electrochemical Immunoassay for Point-of-Care detection of SARS-COV-2 Nucleocapsid protein. Anal. Chem. *94*, 15155–15161. https://doi.org/10.1021/acs.analchem.2c03606.
30. Elgrishi, N., Rountree, K.J., McCarthy, B.D., Rountree, E.S., Eisenhart, T.T., and Dempsey, J.L. (2017). A practical beginner's guide to cyclic voltammetry. J. Chem. Educ. *95*, 197–206. https://doi.org/10.1021/acs.jchemed.7b00361.
31. Wang, H.-W., Bringans, C., Hickey, A.J.R., Windsor, J.A., Kilmartin, P.A., and Phillips, A.R.J. (2021). Cyclic voltammetry in biological samples: A systematic review of methods and techniques applicable to clinical settings. Signals *2*, 138–158. https://doi.org/10.3390/signals2010012.
32. Fan, L., Zhao, G., Shi, H., Liu, M., and Li, Z. (2013). A highly selective electrochemical impedance spectroscopy-based aptasensor for sensitive detection of acetamiprid. Biosens. Bioelectron. *43*, 12–18. https://doi.org/10.1016/j.bios.2012.11.033.
33. Rahmati, Z., Roushani, M., Hosseini, H., and Choobin, H. (2021). Electrochemical immunosensor with Cu2O nanocube coating for detection of SARS-CoV-2 spike protein. Mikrochim. Acta *188*, 105. https://doi.org/10.1007/s00604-021-04762-9.
34. Xu, M., Gao, Z., Wei, Q., Chen, G., and Tang, D. (2015). Hemin/G-quadruplex-based DNAzyme concatamers for in situ amplified impedimetric sensing of copper(II) ion coupling with DNAzyme-catalyzed precipitation strategy. Biosens. Bioelectron. *74*, 1–7. https://doi.org/10.1016/j.bios.2015.05.056.
35. Park, H., Lee, H., Lee, M., Baek, C., Park, J.A., Jang, M., Kwon, Y., Min, J., and Lee, T. (2023). Synthesis of isolated DNA aptamer and its application of AC-electrothermal flow-based rapid biosensor for the detection of dengue virus in a spiked sample. Bioconjugate Chem. *34*, 1486–1497. https://doi.org/10.1021/acs.bioconjchem.3c00249.
36. Yang, F., Yang, Z., Zhuo, Y., Chai, Y., and Yuan, R. (2015). Ultrasensitive electrochemical immunosensor for carbohydrate antigen 19-9 using AU/porous graphene nanocomposites as platform and AU@PD core/shell bimetallic functionalized graphene nanocomposites as signal enhancers. Biosens. Bioelectron. *66*, 356–362. https://doi.org/10.1016/j.bios.2014.10.066.
37. Jolly, P., Miodek, A., Yang, D.K., Chen, L.C., Lloyd, M.D., and Estrela, P. (2016). Electro-Engineered polymeric films for the development of sensitive APTAsensors for prostate cancer marker detection. ACS Sens. *1*, 1308–1314. https://doi.org/10.1021/acssensors.6b00443.
38. Jolly, P., Miodek, A., Yang, D.K., Chen, L.C., Lloyd, M.D., and Estrela, P. (2016c). Electro-Engineered polymeric films for the development of sensitive APTAsensors for prostate cancer marker detection. ACS Sens. *1*, 1308–1314. https://doi.org/10.1021/acssensors.6b00443.
39. Karimi-Maleh, H., Liu, Y., Li, Z., Darabi, R., Orooji, Y., Karaman, C., Karimi, F., Baghayeri, M., Rouhi, J., Fu, L., et al. (2023). Calf thymus ds-DNA intercalation with pendimethalin herbicide at the surface of ZIF-8/Co/rGO/C3N4/ds-DNA/SPCE; A bio-sensing approach for pendimethalin quantification confirmed by molecular docking study. Chemosphere *332*, 138815. https://doi.org/10.1016/j.chemosphere.2023.138815.
40. Naciri, Y., Hsini, A., Ahdour, A., Akhsassi, B., Fritah, K., Ajmal, Z., Djellabi, R., Bouziani, A., Taoufyq, A., Bakiz, B., et al. (2022). Recent advances of bismuth titanate based photocatalysts engineering for enhanced organic contaminates oxidation in water: A review. Chemosphere *300*, 134622. https://doi.org/10.1016/j.chemosphere.2022.134622.
41. Han, S., Chen, C., Chen, C., Wu, L., Wu, X., Lu, C., Zhang, X., Chao, P., Lv, X., Jia, Z., and Hou, J. (2023). Coupling annealed silver nanoparticles with a porous silicon Bragg mirror SERS substrate and machine learning for rapid non-invasive disease diagnosis. Anal. Chim. Acta *1254*, 341116. https://doi.org/10.1016/j.aca.2023.341116.
42. Gawde, K.A., Kesharwani, P., Sau, S., Sarkar, F.H., Padhyé, S., Kashaw, S.K., and Iyer, A.K. (2017). Synthesis and characterization of folate decorated albumin bio-conjugate nanoparticles loaded with a synthetic curcumin difluorinated analogue. J. Colloid Interface Sci. *496*, 290–299. https://doi.org/10.1016/j.jcis.2017.01.092.
43. Zeeshan, F., Madheswaran, T., Panneerselvam, J., Taliyan, R., and Kesharwani, P. (2021). Human serum albumin as multifunctional Nanocarrier for cancer therapy. J. Pharmacol. Sci. (Tokyo, Jpn.) *110*, 3111–3117. https://doi.org/10.1016/j.xphs.2021.05.001.
44. Rabbani, G., and Ahn, S.N. (2019). Structure, enzymatic activities, glycation, and therapeutic potential of human serum albumin: A natural cargo. Int. J. Biol. Macromol. *123*, 979–990. https://doi.org/10.1016/j.ijbiomac.2018.11.053.
45. Uciechowski, P., and Dempke, W.C.M. (2020). Interleukin-6: a masterplayer in the Cytokine network. Oncology *98*, 131–137. https://doi.org/10.1159/000505099.
46. Shang, J., Ye, G., Shi, K., Wan, Y., Luo, C., Aihara, H., Geng, Q., Auerbach, A., and Li, F. (2020). Structural basis of receptor recognition by SARS-CoV-2. Nature *581*, 221–224. https://doi.org/10.1038/s41586-020-2179-y.
47. Walls, A.C., Park, Y.J., Tortorici, M.A., Wall, A., McGuire, A.T., and Veesler, D. (2020). Structure, function, and antigenicity of the SARS-COV-2 spike glycoprotein. Cell *181*, 281–292.e6. https://doi.org/10.1016/j.cell.2020.02.058.
48. Wrapp, D., Wang, N., Corbett, K.S., Goldsmith, J.A., Hsieh, C.L., Abiona, O., Graham, B.S., and McLellan, J.S. (2020). Cryo-EM structure of the 2019-nCoV spike in the prefusion conformation. Science *367*, 1260–1263. https://doi.org/10.1126/science.abb2507.
49. Yan, R., Zhang, Y., Li, Y., Xia, L., Guo, Y., and Zhou, Q. (2020). Structural basis for the recognition of SARS-CoV-2 by full-length human ACE2. Science *367*, 1444–1448. https://doi.org/10.1126/science.abb2762.
50. Khan, M.K., Wang, Q.Y., and Fitzpatrick, M.E. (2016). Atomic Force Microscopy (AFM) for materials characterization. Materials Characterization Using Nondestructive Evaluation (NDE) Methods, 1–16. https://doi.org/10.1016/b978-0-08-100040-3.00001-8.
51. Krieg, M., Fläschner, G., Alsteens, D., Gaub, B.M., Roos, W.H., Wuite, G.J.L., Gaub, H.E., Gerber, C., Dufrêne, Y.F., and Müller, D.J. (2018). Atomic force microscopy-based mechanobiology. Nat. Rev. Phys. *1*, 41–57. https://doi.org/10.1038/s42254-018-0001-7.
52. Nečas, D., and Klapetek, P. (2012). Gwyddion: An open-source software for SPM Data Analysis. Open Phys. *10*. https://doi.org/10.2478/s11534-011-0096-2.
53. Zakashansky, J.A., Imamura, A.H., Salgado, D.F., Romero Mercieca, H.C., Aguas, R.F.L., Lao, A.M., Pariser, J., Arroyo-Currás, N., and Khine, M. (2021). Detection of the SARS-COV-2 spike protein in saliva with shrinky-dink© electrodes. Anal. Methods *13*, 874–883. https://doi.org/10.1039/d1ay00041a.
54. Shrivastava, A., and Gupta, V. (2011). Methods for the determination of limit of detection and limit of quantitation of the analytical methods. Chronicles Young Sci. *2*, 21. https://doi.org/10.4103/2229-5186.79345.

STAR★METHODS

KEY RESOURCES TABLE

REAGENT or RESOURCE	SOURCE	IDENTIFIER
Chemicals, peptides, and recombinant proteins		
CEA human	Sigma-Aldrich	Cat# C4835
Nuclease-free water	Sigma-Aldrich	Cat# W4502-1L
PBS	Sigma-Aldrich	Cat# P4417-100TAB
6-mercapto-1-hexanol (MCH)	Sigma-Aldrich	Cat# 725226-1G
Potassium hexacyanoferrate II	Sigma-Aldrich	Cat# P3289
Potassium hexacyanoferrate III	Sigma-Aldrich	Cat# 244023
Tris(2-carboxyethyl) phosphine (TCEP)	Sigma-Aldrich	Cat# C4706-2G
Human serum	Sigma-Aldrich	Cat# H4522
IL-6	Sigma-Aldrich	Cat# SRP3096
HSA	Sigma-Aldrich	Cat# SRP6182-1MG
SARS-CoV-2 (2019-nCoV) Spike RBD recombinant	Sino Biological	Cat# 40592-VNAH
Oligonucleotides		
CEA aptamer (6): HS-$(CH_4)_6$-OP$(O)_2$O-$(CH_2CH_2O)_6$-5′-TTTTT-GCCAGCGAG TTTTGACCGTTTTTCTCTCTTTTC CGCCTA-3′	Previously selected and characterized by Yunussova et al.[26] and synthesized by Eurogentec	Custom synthesized
Software and algorithms		
Microsoft Excel 2010 v.16.52	Microsoft Office	https://www.microsoft.com/en-us/microsoft-365/previous-versions/microsoft-excel-2010
EIS Spectrum Analyzer v.1.0	Research Institute for Physical-Chemical Problems, Belarusian State University	http://www.abc.chemistry.bsu.by/vi/analyser/
Origin Pro 2016 v.b9.3.2.303	OriginLab Corporation	https://www.originlab.com/index.aspx?go=Support&pid=3224
PSTrace	Metrohm DropSens	N/A
GraphPad Prism v.9.1.0	Prism	https://www.graphpad.com/features
JPK NanoWizard 4XP	Bruker	https://www.bruker.com/en/products-and-solutions/microscopes/bioafm/jpk-nanowizard-4-xp-bioscience.html
Gwyddion	Nečas and Klapetek[52]	http://gwyddion.net
MATLAB	Mathworks	https://www.mathworks.com
MATLAB code to calculate micelle area and micelle circularity	This paper	
Other		
Super sharp high-resolution silicon AFM cantilevers	TipsNano	Cat# NSG30_SS
PalmSens 3 impedance analyzer	PalmSens BV	https://www.palmsens.com/app/uploads/2016/12/PalmSens3-description.pdf
Cable connector for an IDE	Metrohm DropSens	Cat# CACIDEMEA
Block heater, dual control	Stuart, UK	Cat# SBH130DC
UV/ozone cleaner	Bioforce Nanosciences	N/A
Leica DM500 microscope	Leica	N/A
JPK NanoWizard 4XP, an atomic force microscope	Bruker Instruments	N/A

RESOURCE AVAILABILITY

Lead contact

Further information and requests for resources and reagents should be directed to and will be fulfilled by the lead contact, Damira Kanayeva (dkanayeva@nu.edu.kz).

Materials availability

This study did not generate new unique reagents.

Data and code availability

- All data reported in this paper will be shared by the lead contact upon request.
- The MATLAB code used to calculate the micelle area and micelle circularity is available in this paper's supplemental information.
- Any additional information required to reanalyze the data reported in this paper is available from the lead contact upon request.

METHOD DETAILS

Fabrication of the EIS aptasensor and CEA detection

The surface of an IDE was checked for integrity and the absence of any scratches using the Leica DM500 microscope (Leica, Germany). Then, it was thoroughly cleaned with 96% ethanol before being subjected to a UV/ozone for 20 min. Following that, the IDE was washed again with ethanol and left to air-dry before measuring the EIS signal in the redox couple buffer containing 2 mM ferro/ferricyanide $[Fe(CN)_6]^{3-/4-}$ redox couple (potassium hexacyanoferrate II/III) in a 10 mM PBS (pH 7.6). The protocol was adapted from[53] with slight modifications. In brief, a 100 μM of HS-$(CH_6)_6$-$OP(O)_2O$-$(CH_2CH_2O)_6$-5′-TTTTT- CEA aptamer (6) -3′ was dissolved with a reduction buffer (TCEP) at a 1:2 volume ratio for 1 h to reduce the 3′ ends of the aptamer. The solution was subsequently diluted with 10 mM PBS (pH 7.6) to yield 5 μM aptamer final concentration. The aptamer solution was heated for 5 min at 95°C before being placed on ice for 10 min and allowed to cool to room temperature for another 5–7 min. Finally, for the immobilization of aptamer onto the IDE surface, IDE was dipped in an Eppendorf tube containing a 500 μl aptamer solution and incubated at room temperature for 4 h. Following the aptamer incubation, the IDE surface was washed with 10 mM PBS (pH 7.6), and an EIS signal was measured. After the aptamer incubation, the IDE was incubated for 16 h at 4°C with 500 μl of 3 mM MCH diluted in 10 mM PBS (pH 7.6). The stock MCH solution was made with 98% ethanol to a concentration of 10 mM and kept at −20°C until further use. Target CEA (0.002 pg/ml to 2 ng/ml) diluted in a 10 mM PBS (pH 7.6) in a volume of 50 μl was incubated on the IDE surface for 20 min at room temperature. Finally, the electrodes were rinsed in a washing buffer (PBS, 10 mM, pH 7.6). The signal was detected in the redox couple buffer containing 2 mM ferro/ferricyanide $[Fe(CN)_6]^{3-/4-}$ redox couple (potassium hexacyanoferrate II/III) in a 10 mM PBS (pH 7.6). The experimental setup of the method is illustrated in Figure 1.

Electrochemical measurements

Electrochemical measurements were recorded using the PalmSens 3 impedance analyzer equipped with the PSTrace 5.8 software. An IDE was composed of two working electrodes (52 bands, with a band gap and a band width of 10 μm, 4 mm^2 surface area), an auxiliary electrode, and a reference electrode, all manufactured in the same material (gold), on a glass substrate by optical lithography technology. A cable connector was used to connect an IDE to the potentiostat for the EIS measurement (0.1 Hz to 50 kHz with 56 frequencies and 10 mV a.c.) in the redox couple buffer containing 2 mM ferro/ferricyanide $[Fe(CN)_6]^{3-/4-}$ redox couple (potassium hexacyanoferrate II/III) in a 10 mM PBS (pH 7.6). Nyquist plots were fitted to Randle's equivalent circuit using the EIS spectrum analyzer software. CV was performed by scanning the potential from −0.4 to 0.7 V at a scan rate of 0.1 V/s.

Fitting errors of less than 2% were taken for data analysis. All measurements were performed at room temperature inside an in-house-made Faraday cage. All measurements were carried out in triplicate, and the mean value of replicates, standard deviations, and standard errors from the mean were used to report the results.

Optimization studies

An aptamer concentration and a protein incubation time were optimized for the EIS aptasensor development. Detection of 2 pg/ml of CEA in the measurement buffer (10 mM PBS, pH 7.6) was conducted while evaluating the effect of different concentrations (2, 4, 5, and 8 μM) of the CEA aptamer (6). The impact of an incubation time (5, 10, 15, 20, and 25 min) for 2 pg/ml of the target CEA was evaluated, where the IDE surface was functionalized with a 5 μM CEA aptamer (6). All steps were the same as described in Section Fabrication of the EIS aptasensor and CEA detection except for conditions specified in this section.

Specificity study

CEA and non-target proteins such as IL-6, HSA, and SARS-CoV-2 S glycoprotein in a concentration of 7 pg/ml were diluted in a 10 mM PBS (pH 7.6) and were further incubated on the IDE surface for 20 minutes at room temperature. Finally, the electrodes were rinsed in a washing buffer (PBS, 10 mM, pH 7.6), and the signal was detected in the redox couple buffer. IDE surface functionalization steps were the same as described

in Section Fabrication of the EIS aptasensor and CEA detection. 10 mM PBS (pH 7.6) was used as a background. All R_{ct} values were subtracted from the background.

Detection of CEA in serum

Commercially available human serum was diluted 100 times with 100 mM PBS (pH 7.6), and the following CEA concentrations were added into each serum solution: 0.002, 0.02, 0.2, 2, 20, 200, and 2000 pg/ml. After incubating CEA in serum (50 μl) for 20 minutes, the IDE surface was rinsed with 10 mM PBS (pH 7.6), and the electrochemical signals were measured in the redox couple buffer. R_{ct} values of the sample were subtracted from the background that served as serum diluted 100 times in 100 mM PBS (pH 7.6).

AFM study

The surface of electrodes after each treatment stage was imaged using the JPK NanoWizard 4XP, an atomic force microscope with a super sharp probe NSG30_SS. The sensing tip had nominal spring constant $K = 40$ N/m, resonant frequency $f = 320$ kHz, and tip radius $r = 2$ nm. All images were acquired in the air at room temperature, operating in Quantitative imaging (QI™) mode at 1 μm^2 scan size with a 5 nm/pixel resolution. The peak force or set point was 10 nN, and the z-speed was 50 μm/s. JPK-Data processing application software was used to analyze all the acquired images, and histogram operation was applied to obtain root mean square (RMS) roughness. Gwyddion software was used to obtain the representative 3D images.[52] Three independent samples were prepared and imaged for all stages, including the bare IDE, each with at least 15 different sites for statistical analysis. The size and shape of the micelles that were formed on the electrode surface were measured using a custom-written MATLAB code.

QUANTIFICATION AND STATISTICAL ANALYSIS

For each concentration, the percentage in charge transfer resistance was determined using the formula $[(R_{conc\text{-}n} - R_{PBS})/R_{PBS}) \times 100]$ according to the R_{ct} values obtained with the fitting error values less than 2%. All measurements were carried out at least in triplicate, and the mean value of replicates, standard deviations, and standard errors from the mean were used to report the results. $p < 0.05$ values were accepted as significant. The statistical significance of the AFM data obtained was evaluated by the Kruskal-Wallis test, one-way ANOVA, Mann-Whitney test, or unpaired t-test, depending on the test type and the features of each dataset. LOD was calculated using the formula presented in a study.[54]

iScience, Volume *27*

Supplemental information

Rapid detection of carcinoembryonic antigen by means of an electrochemical aptasensor

Nigara Yunussova, Meruyert Tilegen, Tri Thanh Pham, and Damira Kanayeva

Table S1. Analytical performance of selected aptasensors for CEA detection, related to Figure 4

No.	Detection method	Nanomaterial used	Recognition element	Detection range	LOD	Detection time	Reference
1	Electrochemical	AuNPs	Apt1: 3'-SH-ATACCAGCTTATTCAATT-5'; Apt2: 3'-SH-AGGGGGTGAAGGGATACCC-5'	1 to 200 ng/ml	0.5 ng/ml	30 min	[S1]
2	Electrochemical	PEDOT: PSS	5'-NH2-GACGATAGCGGTGACGGCACAGAC GTCCCGCATCCTCCG-3'	0.77 to 14 ng/ml	0.45 ng/ml in a buffer; 1.06 ng/ml in human serum	n/a	[S2]
3	Electrochemical	3D DNT	N1: 5'-AGGGGGTGAAGGGATACCCTTTAATGACGTC GTGACAAAAATGCTGGTGGGTCAATTTATAC CAGCTTATTCAATT-3'; N2: 5'-AGGGGGTGAAGGGATACCCTTTCCGAACGG GTCATAAAAAATCACTCTTGACATCCTTATA CCAGCTTATTCAATT-3'; L1: 5'-ATTGACCCACCAGCAGTGTATGACCCGTTCG GA-3'; L2: 5'-GGATGTCAAGAGTGAGTGGTCACGACGTCAT TA-3'; E1: 5'-SH-TTGATACCAGCTTAT-Fc-3'	10 fg/ml to 50 ng/ml	4.88 fg/ml	40 min	[S3]
4	Electrochemical	lead ion (Pb2+)-dependent DNAzyme, GQDs-IL-NF composite film	HD: 5'-CATCTCTTCTCCGAGCCGGTCGAAATAGTGA GTATACCAGCTTATTCAATTAAG AGA TG-3'; Substrate Chain: 5'- ACTCACTATrAGGAAGA GATG-MB-3'; AD: 5'- CATCTCTTCC-3'	0.5 fg/ml to 0.5 ng/ml	0.34 fg/ml	n/a	[S4]
5	Electrochemical and optical	Zr-MOF, UiO-66 embedded with Ag NCs	5'-$(CH_2)_6$-CCACGATACCAGCTTATTCAATTCGTGG-3'	0.01 to 10 ng/ml (electrochemical); 1-250 ng/ml (SPR)	8.88 pg/ml (electrochemical); 0.3 ng/ml (SPR)	n/a	[S5]
6	Photoelectrochemical	CdTe@CdS core–shell quantum dots (QDs) coupled with exonuclease-I (Exo-I) assisted target recycling	cDNA: 5'-AATTGAATAAGCTGGTATTTTTTT-$(CH_2)_6$-SH-3'; CEA aptamer probe: 5'-NH_2-$(CH_2)_6$-ATA CCA GCT TAT TCA ATT-3'	0.5 pg/ml to 10 ng/ml	0.12 pg/ml	CEA incubation time 1 h	[S6]
7	Electrochemical	GNRs	SH-ATACCAGCTTATTC AATT	0.1 pg/ml to 10 ng/ml	0.05 pg/ml	30 min	[S7]
8	Electrochemical	AuNPs, GQD	Aptamer I: 5'–NH2–ATACCAGCTTATTCAATT–3' CEA; Aptamer II: 5'–NH2–CCCATAGGGAAGTG GGGGA–3'; Hemin aptamer: 5'–NH2–GTGGGTAGGGCGGG TTGG–3'	10.0 fg/ml to 200.0 ng/ml	3.2 fg/ml	CEA incubation time 50 min	[S8]
9	Electrochemiluminescence	magnetic core–shell Fe_3O_4@AuNPs	HP DNA: 5'- CGATAC CAGCTTATTCAATTC CTCAGCGCTGGTATC G-3'; cDNA: 5'-NH_2-TTTTCGATACCA GCTTATTCAATTCCTCATGCTC-SH-3'; Fc DNA: 5'-ATA AGC TGG TAT CG-Fc-3'	10 fg/ml to 10 ng/ml	3.5 fg/ml	n/a	[S9]

10	Electrochemical	n/a	H1: 5'-CATACCAGCTTATTCAATTCAGAATAAGCTGG-3'	10 pg/ml to 100 ng/ml	0.84 pg/ml	n/a	[S10]
11	Electrochemical	n/a	5' SH-$(CH_2)_6$-ATA CCA GCT TAT TCA ATT-3'	1 fg/ml to 1 ng/ml	0.33 fg/ml	CEA incubation time 90 min	[S11]
12	Photoelectrochemical	g-C_3N_4/$CuInS_2$, CoOOH	5'-TTAACTTATTCGACCATATTTTTTTTTT-NH_2-3'; 5'-AGTCTAGGATTCGGCGTGGGTTAATTTTTT-CCCATAGGGAAGTGGGGGA-3'	0.02−40 ng/ml	5.2 pg/ml	several steps of incuabtion	[S12]
13	Electrochemical	n/a	HS-$(CH_6)_6$-$OP(O)_2O$-$(CH_2CH_2O)_6$-5'-TTTTT-GCCAGCGAGTTTTGACCGTTTTTCTCTCTTTTCCGCCTA-3'	2 pg/ml to 2 ng/ml	2.4 pg/ml in a buffer; 3.8 pg/ml in human serum	CEA incubation time 20 min and 2.5 min detection time	this study

AuNPs- gold nanoparticles; HP- Hairpin Probe; Fc-HP3 - Ferrocene-labeled hairpin probe 3; SERS - Surface-enhanced Raman spectroscopy; ECL - Electrochemiluminescence; GQD- Graphene quantum dots; GNRs- Gold nanorods; PDA- Poly-dopamine; PSBMA- poly (sulfobetaine methacrylate); Ag NCs- Silver nanoclusters; Zr-MOF, UiO-66- Zirconium metal–organic framework; GQDs-IL-NF - graphene quantum dot-ionic liquid-Nafion composite film; HD- Hairpin DNA; AD- Auxiliary DNA; 3D DNT- 3D DNA nanoprobe; PEDOT: PSS- graphene and poly (3,4-ethylenedioxythiophene): poly(styrenesulfonate); cDNA - complementary DNA; g-C_3N_4/$CuInS_2$ - copper indium disulfide-sensitized graphitic-like carbon nitride; CoOOH - cobalt oxyhydroxide.

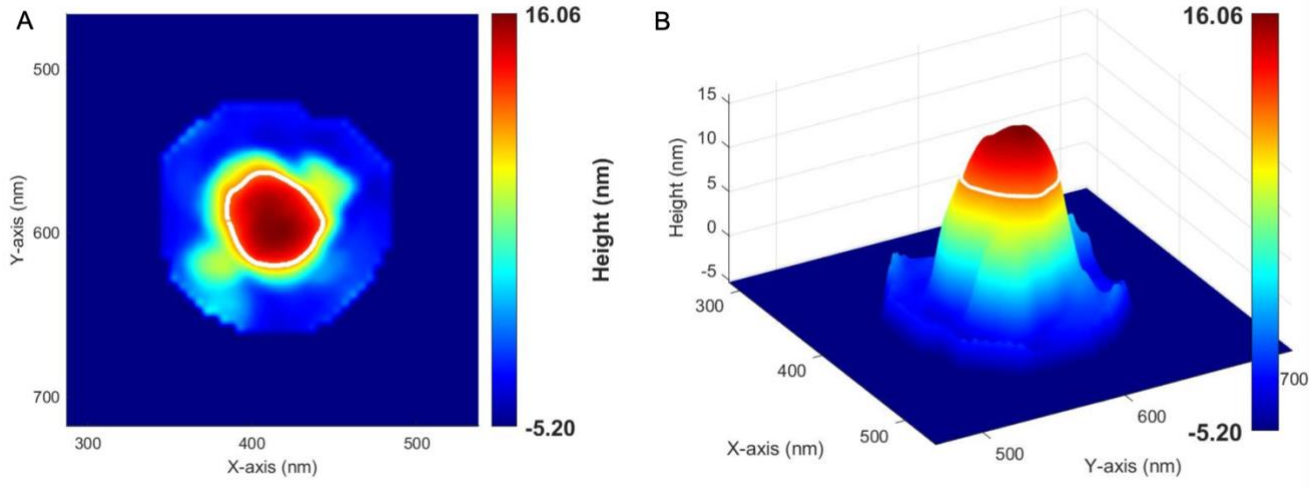

Figure S1. Typical images of a micelle on the electrode surface, related to Figure 5

In both 2D **(A)** and 3D **(B)** images, the white ring around the micelle denoted the chosen micelle perimeter at 75% of its height.

References

1. Shu, H., Wen, W., Xiong, H., Zhang, X., and Wang, S. (2013). Novel electrochemical aptamer biosensor based on gold nanoparticles signal amplification for the detection of carcinoembryonic antigen. Electrochemistry Communications, 37, 15-19. 10.1016/j.elecom.2013.09.018.

2. Yen, Y., Chao, C., and Yeh, Y. (2020). A Graphene-PEDOT: PSS Modified Paper-Based Aptasensor for Electrochemical Impedance Spectroscopy Detection of Tumor Marker. Sensors, 20(5), 1372. 10.3390/s20051372.

3. Ji, Y., Guo, J., Ye, B., Peng, G., Zhang, C., and Zou, L. (2022). An ultrasensitive carcinoembryonic antigen electrochemical aptasensor based on 3D DNA nanoprobe and Exo III. Biosensors and Bioelectronics, 196, 113741. 0.1016/j.bios.2021.113741.

4. Huang, J., Zhao, L., Wan, L., Wen, W., Wang, Y., Bao, T., Wang, S. (2018). A high-sensitivity electrochemical aptasensor of carcinoembryonic antigen based on graphene quantum dots-ionic liquid-nafion nanomatrix and DNAzyme-assisted signal amplification strategy. Biosensors and Bioelectronics, 99, 28–33. 10.1016/j.bios.2017.07.036.

5. Guo, C., Su, F., Song, Y., Hu, B., Wang, M., and He, L. et al. (2017). Aptamer-Templated Silver Nanoclusters Embedded in Zirconium Metal–Organic Framework for Bifunctional Electrochemical and SPR Aptasensors toward Carcinoembryonic Antigen. ACS Applied Materials &Amp; Interfaces, 9(47), 41188-41199. 10.1021/acsami.7b14952.

6. Cong, X., Fan, G.-C., Wang, X., Abdel-Halim, E. S., and Zhu, J.-J. (2016). Enhanced photoelectrochemical aptasensing platform amplified through the sensitization effect of CdTe@CdS core–shell quantum dots coupled with exonuclease-I assisted Target Recycling. Journal of Materials Chemistry B, 4(36), 6117–6124. 10.1039/c6tb01807f.

7. Si, Z., Xie, B., Chen, Z., Tang, C., Li, T., and Yang, M. (2017). Electrochemical aptasensor for the cancer biomarker CEA based on aptamer induced current due to formation of molybdophosphate. Mikrochimica Acta, 184(9), 3215–3221. 10.1007/s00604-017-2338-5.

8. Shekari, Z., Zare, H. R., and Falahati, A. (2019) Electrochemical sandwich aptasensor for the carcinoembryonic antigen using graphene quantum dots, gold nanoparticles and nitrogen doped graphene modified electrode and exploiting the peroxidase-mimicking activity of a G-quadruplex DNAzyme. Microchimica Acta 186. 10.1007/s00604-019-3572-9.

9. Jie, G., Ge, J., Gao, X., and Li, C. (2018). Amplified electrochemiluminescence detection of CEA based on magnetic Fe3O4@Au nanoparticles-assembled Ru@SiO2 nanocomposites combined with multiple cycling amplification strategy. Biosensors and Bioelectronics, 118, 115–121. 10.1016/j.bios.2018.07.046.

10. Niu, C., Lin, X., Jiang, X., Guo, F., Liu, J., Liu, X., Huang, Y. (2022). An electrochemical aptasensor for highly sensitive detection of CEA based on Exonuclease III and hybrid chain reaction dual signal amplification. Bioelectrochemistry, 143, 107986. 10.1016/j.bioelechem.2021.107986.

11. Xie, Y., Guan, Z., Ma, H., Wang, P., and Xi, S. (2023). Ultrasensitive detection of carcinoembryonic antigen based on exonuclease iii-assisted recycling and hybridization Chain

Reaction Strategies. International Journal of Electrochemical Science, 18(5), 100127. 10.1016/j.ijoes.2023.100127.

12. Zhang, K., Lv, S., Zhou, Q., and Tang, D. (2020). CoOOH nanosheets-coated g-C3N4/CuInS2 nanohybrids for photoelectrochemical biosensor of carcinoembryonic antigen coupling hybridization chain reaction with etching reaction. Sensors and Actuators B: Chemical, 307, 127631.10.1016/j.snb.2019.127631.